Eclipta Journals



RESEARCH

Entropy-Stable Differentiable Simulation for Dissolution-Affected Gas Influx in Drilling Annuli with Adjoint-Based Calibration

Rizal Mendoza[1] and Alvin Bautista[2]

[1]Central Mindanao University, University Town, Musuan, Maramag 8710, Philippines
[2]West Visayas State University, Luna Street, La Paz, Iloilo City 5000, Philippines

Abstract

Drilling hydraulics operated near narrow pressure margins require models that are simultaneously fast, numerically robust, and physically consistent under strong compressibility and transient actuation. Managed pressure drilling amplifies this requirement because choke and pump actions can generate pressure waves and flow reversals that interact with multiphase transport and with thermodynamic gas dissolution into oil-based or synthetic-based fluids. Dissolution-driven swelling modifies the effective liquid volume and density, reshaping pit-volume and pressure signatures and complicating interpretation of early influx events. This paper develops a thermodynamically consistent, entropy-stable, and differentiable annular simulator that couples one-dimensional transient transport with a bounded dissolution and swelling closure. The technical contribution is a discrete formulation that enforces positivity of phase fractions and densities, satisfies a provable discrete entropy inequality under time-dependent boundary actuation, and remains differentiable end-to-end through implicit source updates. Differentiability enables continuous-adjoint calibration of uncertain friction, slip, sensor bias, and dissolution-kinetic parameters from streaming surface measurements, while entropy stability prevents unphysical oscillations that can corrupt gradient-based inversion. The simulator uses an invariant-region-preserving flux with well-balanced hydrostatics, an IMEX operator split for dissolution, and an implicit-function-theorem treatment of stiff thermodynamic updates to provide stable gradients. Numerical studies show that entropy-stable discretization reduces spurious pit-gain transients and prevents gradient blow-up under aggressive choke maneuvers, yielding tighter parameter posteriors and more reliable early-event classification when swelling competes with free-gas expansion.

1. Introduction

Real-time interpretation of drilling signals is constrained by two realities that do not align neatly with simplified modeling assumptions [1]. The first reality is that the annulus is a distributed, compressible, and strongly forced system: pump ramps, choke adjustments, and density changes create pressure transients that propagate faster than the transport time scale of migrating gas. The second reality is that the most actionable measurements are surface-based and aggregated, such as pit volume change, flow-out, and pressure at a small number of points. The mismatch between distributed dynamics and aggregated sensing means that a model used for inference must be robust under partial observability and under input-driven transients, rather than merely accurate in nominal steady conditions. This requirement is intensified in managed pressure drilling, where control actions are not occasional interventions but continuous manipulations of boundary conditions, and where the actuation itself modifies the signatures used to decide whether an influx is occurring [2].

Gas influx interpretation becomes materially more ambiguous when a significant fraction of gas dissolves into the circulating fluid. In oil-based and synthetic-based muds, dissolution can be non-negligible at elevated pressures, and the dissolved inventory can change as pressure evolves along the annulus. Dissolved gas can induce swelling, changing effective liquid volume and density and thereby altering both hydrostatics and surface volumetric balances. This can produce early pit-volume changes without an equivalently large free-gas holdup, and it can delay or soften the appearance of a distinct gas phase at the surface. The resulting observability problem is not simply that gas is hidden, but that the system's constitutive behavior is modified by the hidden inventory, so the model must represent dissolution and swelling as internal state rather than as an output correction [3]. Manikonda et al. (2020) and Manikonda et al. (2021) presented a first thermodynamic modeling approach for estimating gas-kick dissolution effects in oil-based drilling fluids, linking pressure-dependent solubility to swelling behavior relevant for pit-volume interpretation [4] [5]. That framing motivates the present paper's choice to embed dissolu-

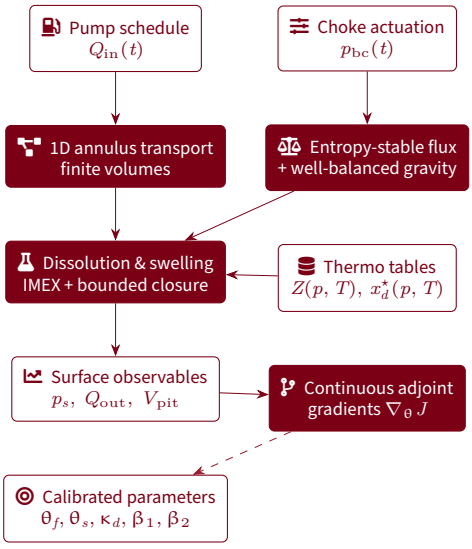


Figure 1. End-to-end differentiable annular simulator: entropy-stable transport and well-balanced hydrostatics feed a bounded dissolution–swelling closure; surface predictions drive adjoint gradients for calibrating friction, slip, dissolution kinetics, swelling coefficients, and sensor biases.

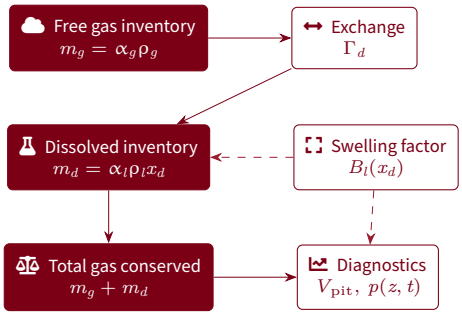


Figure 2. State decomposition for dissolution-affected influx: free and dissolved gas inventories exchange via a bounded kinetic term while conserving total gas; swelling modifies liquid density through $B_l(x_d)$, reshaping hydrostatics and pit-volume/flow-out signatures.

tion and swelling directly in the dynamical model and, critically, to do so in a way that is compatible with numerical stability and with gradient-based calibration.

Even when dissolution is represented mechanistically, predictive uncertainty remains dominated by fluid-property and friction uncertainties that compound along the annulus [6]. Gas density, viscosity, and compressibility influence both hydrostatic distributions and frictional pressure losses, and small errors in these properties can induce systematic mismatch between predicted and measured pressures. Those mismatches then contaminate any inferred influx rate or depth because the inference algorithm uses the model to attribute residuals to hidden states. Sleiti et al. (2021) evaluated several property correlations used in kick-related calculations and reported residual errors that remain at a few percent level even for comparatively accurate formulations in high-temperature and high-pressure regimes, including gas-viscosity correlation performance spanning roughly 3.50% to 4.45% average absolute relative error for density-based models under the evaluated conditions [7]. For real-time transient inference, such residual errors can be amplified by compressibility and by boundary actuation, making it difficult to maintain stable estimation unless the numerical method itself is robust and unless uncertain parameters can be calibrated consistently from data.

A further and often under-appreciated barrier arises when model-based inference relies on differentiable programming, adjoint methods, or other gradient-based approaches [8]. Differentiability is attractive because it can dramatically reduce computational cost relative to ensemble-based or derivative-free estimation, especially when the parameter dimension is moderate and when streaming updates are required. However, naive differentiation through stiff source terms, positivity projections, or non-smooth numerical flux limiters can yield unstable gradients that are not physically meaningful. Gradient blow-up frequently occurs precisely in the regimes that matter most operationally: near phase

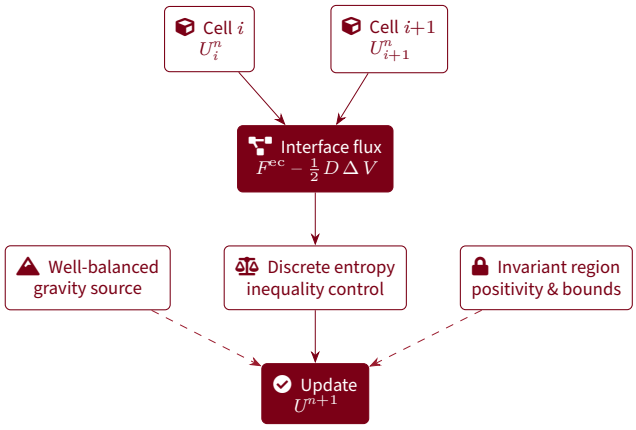


Figure 3. Entropy-stable finite-volume transport step: an entropy-conservative core flux plus smooth dissipation yields a discrete entropy bound, while well-balanced gravity and invariant-region handling maintain hydrostatic consistency and physically admissible states during transients.

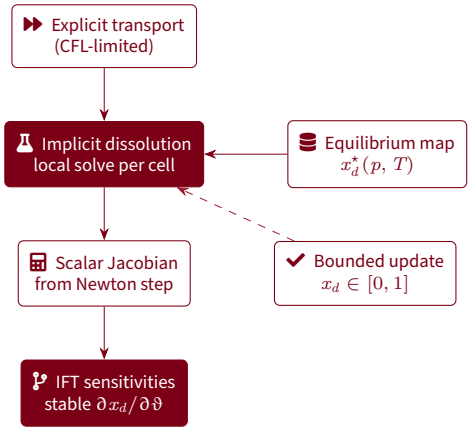


Figure 4. IMEX source handling for stiff dissolution: transport advances explicitly, while a local implicit update enforces bounded thermodynamics; implicit-function-theorem sensitivities reuse the scalar Jacobian to deliver stable gradients without iteration-dependent differentiation.

appearance, during rapid boundary actuation, and under near-equilibrium dissolution where small state changes produce large implied mass transfers. In such regimes, a simulator that is stable in the forward sense can still be unstable in the sensitivity sense, undermining calibration and any downstream decision logic built on inferred parameters [9].

This paper addresses these coupled difficulties by developing a simulator that is designed around three properties rather than around a single fidelity target. The first property is thermodynamic consistency under dissolution and swelling, expressed through bounded equilibrium mappings and a mass-conserving exchange term that does not create or destroy gas inventory. The second property is entropy stability in the sense of a discrete inequality that controls numerical oscillations under transient forcing and preserves an invariant region for physically admissible states, including positivity of density and boundedness of phase fractions. The third property is differentiability that remains well behaved under stiff source updates, achieved through an IMEX split and an implicit-function-theorem treatment of the implicit step so that gradients reflect the true local sensitivity of the discrete update rather than the artifacts of a projection or a clipped limiter.

The thesis of the paper is that entropy stability and differentiability are not competing objectives for this class of drilling hydraulics problems, but mutually reinforcing constraints that together enable reliable adjoint-based calibration in dissolution-affected influx scenarios [10]. Entropy stability regularizes the forward solution in precisely the regimes where gradients would otherwise become pathological, while differentiability enables systematic parameter and bias calibration so that property and closure uncertainty can be reduced online rather than absorbed implicitly into hidden influx estimates. The resulting combination yields a model that is not merely a simulator but an inference engine: it provides stable forward predictions, stable sensitivities, and consistent parameter updates.

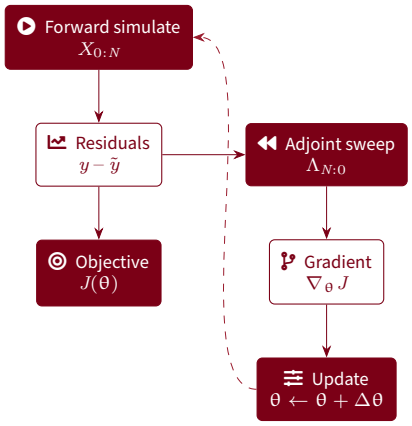


Figure 5. Adjoint-based calibration loop: forward trajectories produce multi-sensor residuals, a backward adjoint sweep computes gradients efficiently, and smooth parameter updates refine friction, slip, dissolution/swelling, and bias parameters for stable real-time inference.

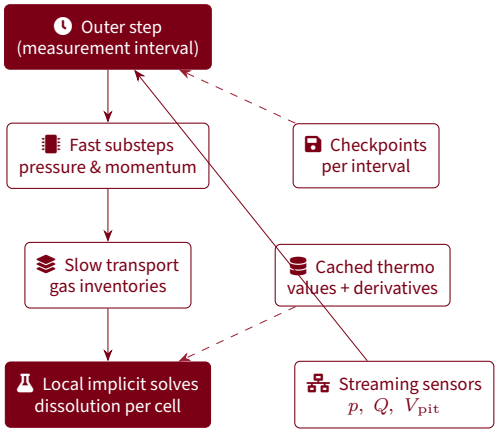


Figure 6. Real-time multirate structure: fast substeps resolve actuation-driven pressure dynamics, slower conservative transport advances inventories, and local implicit dissolution updates run efficiently with cached thermodynamic evaluations and interval checkpointing for adjoint recomputation.

The remainder of the paper develops this thesis. A modeling section formulates the annular dynamics with a dissolution and swelling closure chosen to be bounded and differentiable [11]. A numerical section derives an entropy-stable and invariant-region-preserving discretization with well-balanced hydrostatics and a stiffly stable source update. A calibration section presents a continuous-adjoint formulation for parameter and bias estimation and discusses how the discrete entropy structure improves adjoint conditioning. A computational section describes multirate implementation choices and differentiable implicit solves for real-time feasibility. A numerical section reports studies focusing on transient boundary actuation, early influx ambiguity under swelling, and the stability of gradients used for calibration. The paper concludes with implications and limitations [12].

2. Dynamical Model with Dissolution, Swelling, and Bounded Thermodynamics

A control-relevant annular model must predict how boundary actuation and influx sources shape bottomhole pressure, surface pressures, flow-out, and pit-volume dynamics. The present formulation adopts a one-dimensional representation along the annulus coordinate $z \in [0, L]$, discretized later into finite volumes. The state variables are chosen to support both thermodynamic closure and conservative transport. A mixture-based representation is used for momentum, while mass is tracked separately for free gas, liquid, and dissolved gas in the liquid [13].

Let $\alpha_g(z,t)$ be the free-gas volume fraction and $\alpha_l(z,t) = 1 - \alpha_g(z,t)$ the liquid volume fraction. Let $\rho_g(z,t)$ and $\rho_l(z,t)$ denote gas and liquid densities, and let $u_g(z,t)$ and $u_l(z,t)$ denote their velocities. A dissolved gas mass fraction in the liquid, denoted $x_d(z,t)$, is introduced as an internal scalar state. The total gas inventory per unit volume is then $\alpha_g\rho_g + \alpha_l\rho_l x_d$. This

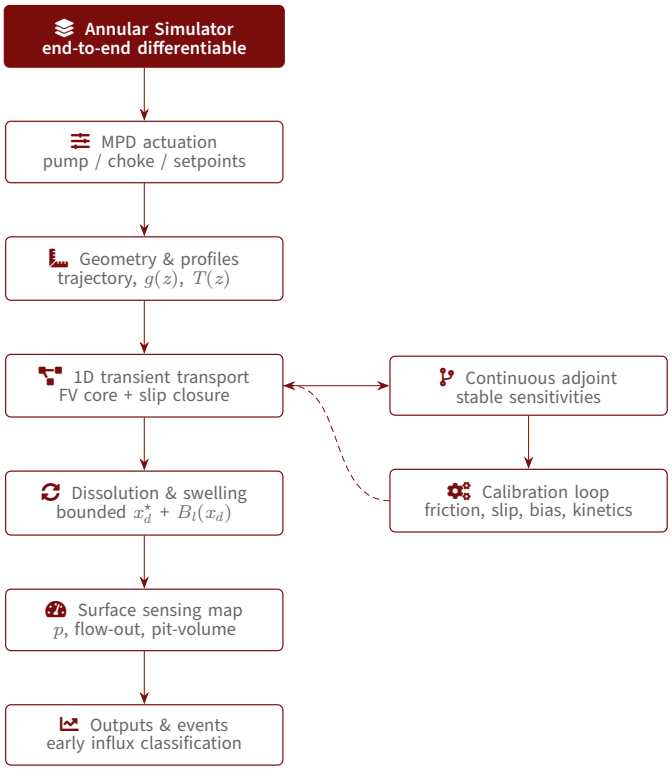


Figure 7. High-level architecture of the entropy-stable differentiable annular simulator. Boundary actuation and geometry feed a finite-volume transport core, coupled to bounded dissolution and swelling closures. A differentiable sensing map produces pressure/flow/pit signals, while a continuous-adjoint calibration loop updates uncertain friction, slip, dissolution-kinetic, swelling, and bias parameters to keep inference stable under aggressive MPD transients.

decomposition is essential because the observable impact of gas depends strongly on whether the gas is free, affecting compressibility and slip, or dissolved, affecting swelling and density [14].

The free-gas mass balance and dissolved-gas balance can be written as conservative transport with exchange,

$$\begin{aligned} \partial_t(\alpha_g \rho_g) + \partial_z(\alpha_g \rho_g u_g) &= s_k(z,t) - \Gamma_d \\ \partial_t(\alpha_l \rho_l x_d) + \partial_z(\alpha_l \rho_l x_d u_l) &= \Gamma_d \end{aligned} \tag{1}$$

where $s_k(z,t)$ represents a potential influx source localized near an unknown depth and onset time, and Γ_d is the net dissolution rate transferring gas mass between free and dissolved inventories. The liquid mass equation can be written similarly, but for many managed pressure drilling scenarios it is sufficient to treat the liquid mass flux as driven primarily by circulation and to represent density changes through swelling and compressibility, provided that the conservative gas inventory equations are maintained.

Momentum is represented at the mixture level to avoid the stiffness and data requirements of a full two-fluid momentum closure, while still capturing the primary coupling between pressure gradients, hydrostatics, and friction [15]. Define mixture density $\rho_m = \alpha_g \rho_g + \alpha_l \rho_l$ and mixture velocity $u_m = \alpha_g u_g + \alpha_l u_l$. A compressible mixture momentum balance is modeled as

$$\partial_t(\rho_m u_m) + \partial_z(\rho_m u_m^2 + p) = -\rho_m g(z) - \tau_f(z,t) \tag{2}$$

where $p(z,t)$ is pressure, $g(z)$ is gravitational acceleration projected along the well trajectory, and τ_f is an effective friction term that aggregates wall shear and interfacial contributions. For differentiable calibration, τ_f is parameterized by a small set of coefficients, such as a friction multiplier and a flow-regime smoothing parameter, so that gradients can identify how friction should shift to match measured standpipe pressure and surface pressures. The parameterization is chosen to be smooth in u_m to avoid non-differentiability at flow reversal [16].

Phase velocities are closed through a slip relation. The model uses a drift form,

$$u_g = u_m + V_s(\alpha_g, p, T; \theta_s) \tag{3}$$

with V_s a slip velocity closure controlled by parameters θ_s. The intent is to represent the tendency of gas to rise relative to liquid and to capture how gas migration timing affects surface gas fraction and pressure transients. The closure is kept differentiable by using smooth saturation functions rather than piecewise regime switches, which improves adjoint conditioning

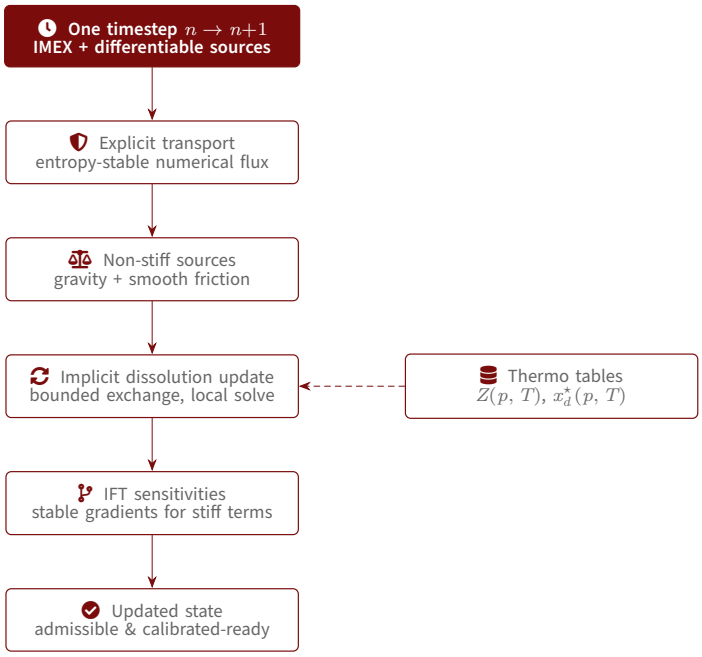


Figure 8. IMEX update structure used to keep dissolution exchange stable without sacrificing end-to-end differentiability. Entropy-stable explicit transport and smooth non-stiff sources advance conservative inventories, followed by a local implicit dissolution/swelling solve. Implicit-function-theorem sensitivities reuse the local Jacobian to provide gradients that remain bounded under near-equilibrium dissolution and rapid boundary actuation.

Table 1. Model state variables.

Symbol	Meaning	Units
$\alpha_g(z,t)$	Free gas vol. frac.	–
$\alpha_l(z,t)$	Liquid vol. frac.	–
$\rho_g(z,t)$	Gas density	kg/m^3
$\rho_l(z,t)$	Liquid density	kg/m^3
$u_g(z,t)$	Gas velocity	m/s
$u_l(z,t)$	Liquid velocity	m/s
$x_d(z,t)$	Dissolved-gas mass frac.	–

at the cost of some regime sharpness that is typically unidentifiable from surface data anyway [17].

The thermodynamic closure links pressure and temperature to gas density, equilibrium solubility, and swelling. Gas density is represented as a real-gas mapping,

$$\rho_g(p,T) = \frac{pM_g}{Z(p,T)RT} \tag{4}$$

where M_g is an effective molar mass, R is the universal gas constant, and $Z(p,T)$ is a compressibility factor. The function Z is evaluated through a differentiable table interpolation or a smooth surrogate that preserves monotonicity and boundedness [18]. This choice is motivated by operational needs: a full equation-of-state solve at each cell and time step is unnecessary for the present objectives, but the model must preserve the correct dependence of density on pressure to avoid spurious wave speeds and incorrect hydrostatics.

Equilibrium dissolved fraction is modeled as $x_d^\star(p,T)$, again evaluated through a differentiable mapping. Dissolution kinetics are modeled by relaxation toward equilibrium,

$$\Gamma_d = \kappa_d\,\alpha_l\rho_l\big(x_d^\star(p,T) - x_d\big) \tag{5}$$

where κ_d is an effective mass-transfer coefficient representing mixing and interfacial area. This relaxation form is not intended as a detailed interfacial model; it is chosen because it preserves conservation of total gas inventory, it is bounded, and it admits stiffly stable implicit updates [19]. The sign of Γ_d naturally switches when the local dissolved fraction exceeds equilibrium, representing exsolution under depressurization and dissolution under pressurization.

Swelling is represented as a modification of liquid specific volume and density. Let $\rho_{l,0}(T)$ be a base liq-

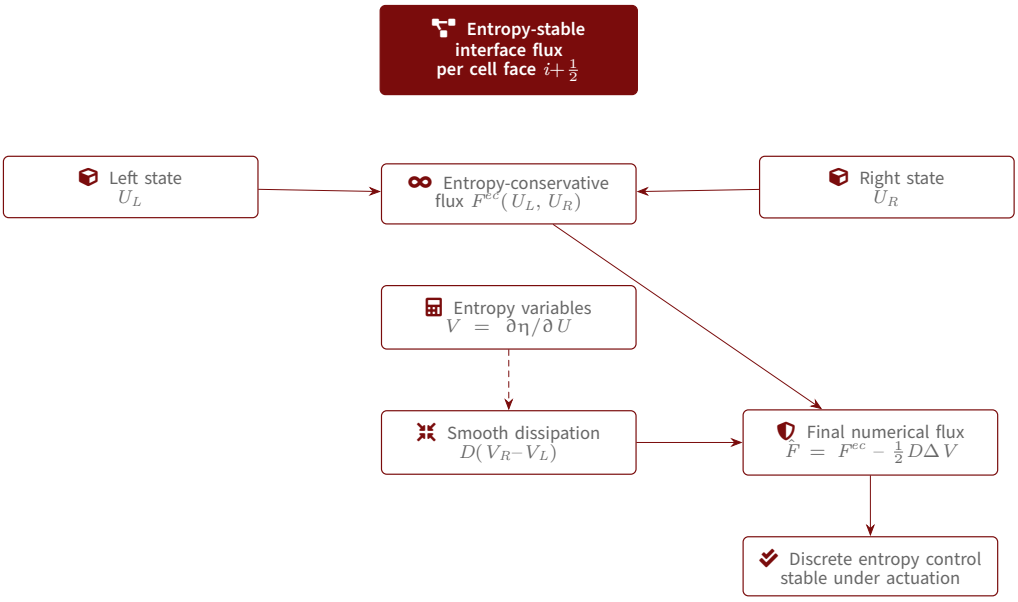


Figure 9. Construction of an entropy-stable finite-volume interface flux used to damp nonphysical oscillations while retaining sharp, actuation-driven transients. An entropy-conservative core flux is augmented with a smooth dissipation operator formulated in entropy variables, avoiding non-differentiable sign changes under flow reversal and improving adjoint conditioning for calibration.

Table 2. Gas inventory and dissolution closures.

Term	Definition	Note
m_g	$\alpha_g \rho_g$	Free-gas mass density
m_d	$\alpha_l \rho_l x_d$	Dissolved-gas mass density
$x_d^\star$	$x_d^\star(p, T)$	Equilibrium solubility
Γ_d	$\kappa_d \alpha_l \rho_l (x_d^\star - x_d)$	Exchange, $m_g + m_d$ conserved
B_l	$1 + \beta_1 x_d + \beta_2 x_d^2$	Swelling factor, $B_l \geq 1$
ρ_l	$\rho_{l,0}(T)/B_l$	Swelling-modified density

uid density in the absence of dissolved gas. Define a swelling factor $B_l(p, T, x_d)$ such that

$$\rho_l(p, T, x_d) = \frac{\rho_{l,0}(T)}{B_l(p, T, x_d)} \tag{6}$$

with $B_l \geq 1$ [20]. A bounded polynomial form in x_d is used for differentiability and for calibration,

$$B_l = 1 + \beta_1 x_d + \beta_2 x_d^2 \tag{7}$$

where β_1 and β_2 are parameters that can be calibrated within physically plausible bounds. This representation captures the practical effect that swelling increases with dissolved fraction and does so nonlinearly, while remaining smooth. The key point is that swelling changes volume without creating mass, and the present formulation maintains that principle by computing volumetric quantities diagnostically from mass and density rather than updating volume directly.

Pit-volume change and surface flow-out are modeled through boundary fluxes and through the density-dependent mapping from mass flow to volumetric flow [21]. The pit-volume dynamic is expressed as an integral of net volumetric imbalance,

$$\frac{dV_{\text{pit}}}{dt} = Q_{\text{in}}(t) - Q_{\text{out}}(t) \tag{8}$$

where Q_{out} depends on return mass flux and swollen density. This is precisely the mechanism by which dissolution-driven swelling can produce pit gain even when free-gas holdup is small. In such regimes, a model that does not represent x_d can attribute pit gain incorrectly to free gas, leading to biased inferred gas holdup and to incorrect predictions of surface gas handling.

Boundary conditions represent managed pressure drilling actuation [22]. At the surface, choke behavior imposes a relation between outflow and backpressure, expressed as a smooth function to preserve differentiability. At the inlet, pump rate sets inflow mass or volumetric flux. The model also supports time-dependent casing pressure setpoints and can represent valve dynamics through a first-order lag if needed, again chosen to be smooth.

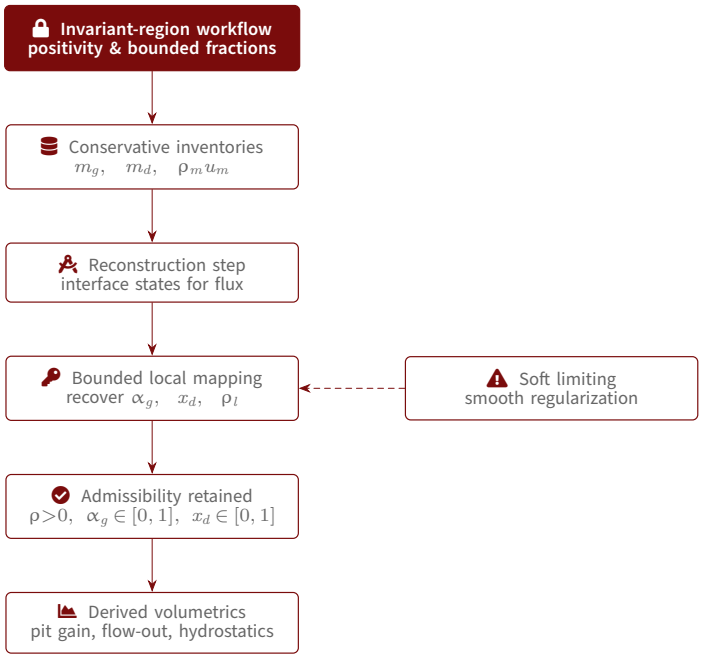


Figure 10. Invariant-region preservation strategy used to prevent unphysical states without non-differentiable clipping. The scheme advances conservative inventories, reconstructs interface states, then applies a bounded local mapping to recover phase fractions and swollen liquid density. Smooth limiting is reserved for rare edge cases, keeping gradients consistent for adjoint-based calibration.

Table 3. Mixture and momentum representations.

Quantity	Expression	Role
ρ_m	$\alpha_g\rho_g + \alpha_l\rho_l$	Mixture density
u_m	$\alpha_g u_g + \alpha_l u_l$	Mixture velocity
u_g	$u_m + V_s(\alpha_g, p, T; \theta_s)$	Slip closure
Momentum flux	$\rho_m u_m^2 + p$	Convective + pressure
Momentum source	$-\rho_m g(z) - \tau_f(z,t)$	Gravity and friction

The resulting continuous model is a coupled nonlinear balance law with a stiff source term in the dissolution exchange when κ_d is large. It also contains a delicate coupling between density, pressure, and phase fraction that can generate numerical oscillations during transients [23]. These challenges motivate the numerical design in the next section, which constructs a discretization that is entropy stable and invariant-region preserving while remaining differentiable.

3. Entropy-Stable Discretization and Invariant-Region Preservation

Forward stability is a prerequisite for reliable inference, but in this setting forward stability alone is insufficient. A simulator that produces bounded outputs can still produce unphysical oscillations near phase appearance or rapid actuation, and those oscillations can severely distort gradients used for calibration. The numerical method therefore targets an entropy stability property that controls oscillations through a discrete inequality, together with invariant-region preservation that ensures positivity and boundedness of key states [24]. The construction is developed in the finite-volume setting to preserve conservation of mass and to enable well-defined fluxes under discontinuities.

Let $U(z,t)$ denote the vector of conserved and quasi-conserved variables selected for discretization. A representative choice includes mixture mass, mixture momentum, free-gas mass, and dissolved-gas mass. In compact form, the continuous dynamics can be written as

$$\partial_t U + \partial_z F(U) = S(U;\theta) \tag{9}$$

where $F(U)$ is the advective flux and $S(U;\theta)$ collects gravity, friction, influx sources, and dissolution exchange terms parameterized by θ [25]. The discretization partitions the annulus into cells indexed by i with centers z_i and interfaces $z_{i\pm1/2}$. The finite-volume update is

$$U_i^{n+1} = U_i^n - \frac{\Delta t}{\Delta z}\left(\hat{F}_{i+1/2}^n - \hat{F}_{i-1/2}^n\right) + \Delta t\, S_i^{n+1/2} \tag{10}$$

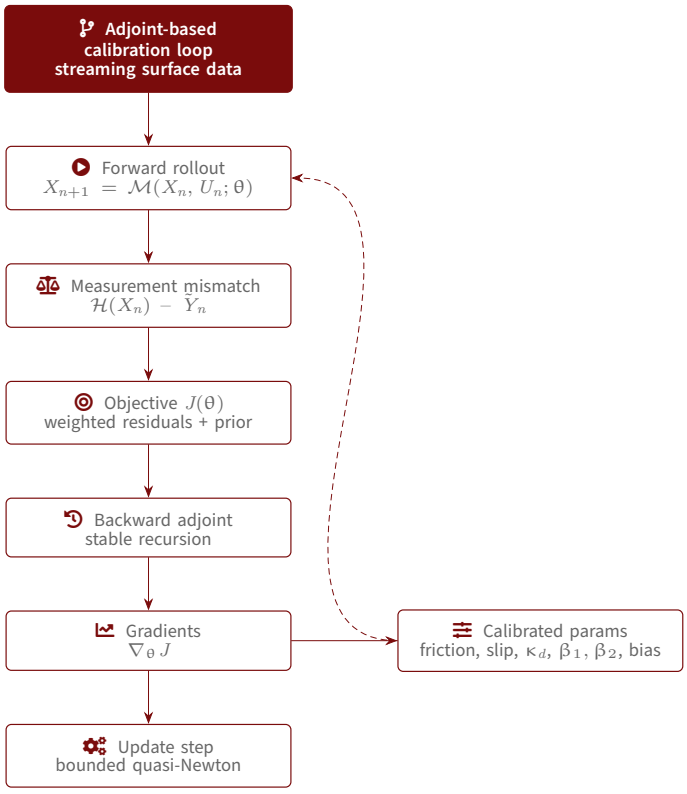


Figure 11. Calibration loop enabled by differentiable IMEX updates and entropy-stable transport. Forward simulation produces predicted surface signals; residuals form an objective with regularization; a backward adjoint computes gradients efficiently for multiple parameters. Updated parameters feed back into the simulator to reduce systematic mismatch and improve early-event interpretation when swelling competes with free-gas expansion.

Table 4. Entropy-stable discretization ingredients.

Component	Choice	Aim
Numerical flux	Entropy-conservative F^{ec} + dissipation	Discrete entropy inequality
Dissipation	$D_{i+1/2}(U_L, U_R)(V_R - V_L)$	Wave-based, smooth in states
Entropy variables	$V = \partial\eta/\partial U$	Symmetrization and metric
Gravity source	Well-balanced discretization	Preserve hydrostatic states
Limiter	Smooth slope limiting	Reduce ringing, keep gradients

with numerical fluxes $\hat{F}$ and source approximation $S_i^{n+1/2}$. Entropy stability is achieved by selecting fluxes and source discretization such that a discrete entropy inequality holds for a convex entropy function $\eta(U)$.

An entropy pair (η, q) satisfies, for the continuous system without sources, $\partial_t \eta(U) + \partial_z q(U) \le 0$ in the presence of physical dissipation. For compressible flow-like systems, η can be chosen as a negative of physical entropy or as an energy-like quantity [26]. In annular multiphase systems with closures, the entropy selection is not unique, but an energy-based entropy that penalizes kinetic energy and compressibility and that remains convex in a suitable variable set is sufficient for numerical stabilization. The discrete entropy inequality takes the form

$$\eta(U_i^{n+1}) \le \eta(U_i^n) - \frac{\Delta t}{\Delta z}\left(\hat{q}_{i+1/2}^n - \hat{q}_{i-1/2}^n\right) + \Delta t \Sigma_i^n \quad (11)$$

where $\hat{q}$ is a numerical entropy flux consistent with $\hat{F}$ and Σ_i^n accounts for entropy production by sources such as friction. Achieving this inequality in practice motivates the use of entropy-stable fluxes constructed from entropy-conservative fluxes plus a dissipation operator that is scaled by wave speeds and that is symmetric positive semidefinite in entropy variables.

A practical entropy-stable flux for the present application is constructed as

$$\hat{F}_{i+1/2} = F^{\mathrm{ec}}(U_L, U_R) - \frac{1}{2} D_{i+1/2}(U_L, U_R)\left(V_R - V_L\right) \quad (12)$$

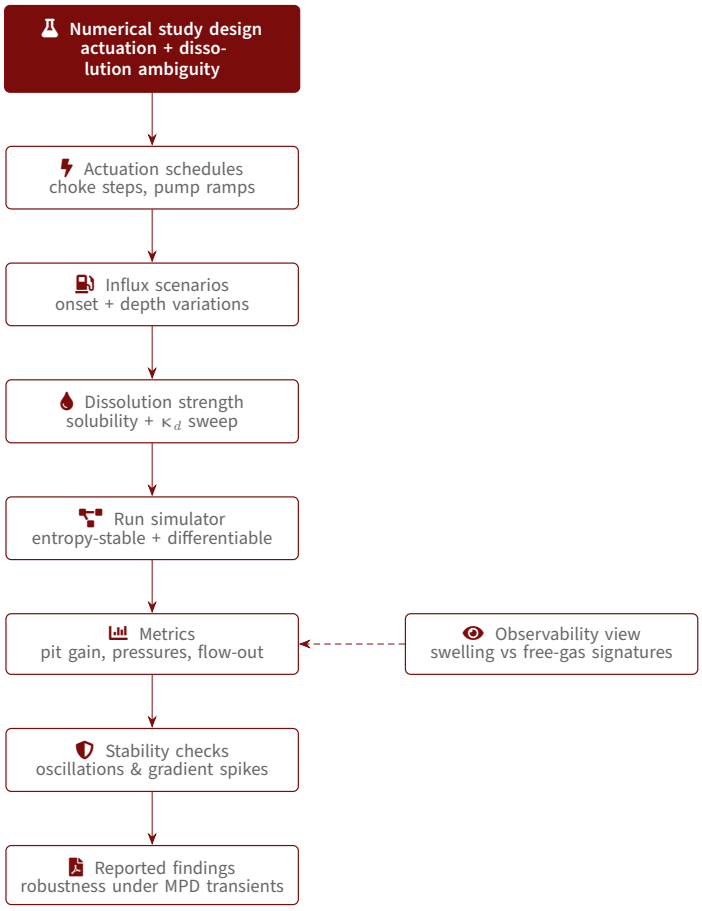


Figure 12. Compact study map used to stress-test the proposed method where inference is hardest: fast choke/pump actuation, early influx with strong dissolution, and regimes where swelling reshapes pit-volume signatures. The evaluation emphasizes both forward robustness (suppressed numerical ringing) and sensitivity robustness (bounded adjoint gradients) to support reliable online calibration.

where F^{ec} is an entropy-conservative flux, $V = \partial\eta/\partial U$ are entropy variables, and $D_{i+1/2}$ is a dissipation matrix chosen to satisfy entropy stability. The dissipation can be based on an approximate Riemann solver wave speed estimate. For differentiability, $D_{i+1/2}$ is made a smooth function of states through smooth absolute-value approximations of eigenvalues, avoiding non-differentiability at sign changes that occur under flow reversal.

Hydrostatic well-balancing is important because drilling hydraulics often operates near hydrostatic equilibrium with small dynamic deviations. If gravity source terms are discretized inconsistently with fluxes, the method can generate spurious velocities and pressure oscillations that then contaminate pit and pressure signals. The scheme therefore uses a well-balanced source discretization that exactly preserves discrete hydrostatic equilibrium for the liquid-dominated state. This is achieved by splitting pressure into hydrostatic and dynamic parts and ensuring that the discrete pressure gradient and gravity terms cancel at equilibrium. The cancellation is maintained under swelling-modified density by treating density consistently in both flux and source terms [27].

Invariant-region preservation ensures that physically admissible states remain admissible at the discrete level. The relevant invariant region includes positivity of ρ_g and ρ_l, boundedness of α_g in $[0, 1]$, and boundedness of x_d in $[0, 1]$. Positivity of densities is maintained by evolving logarithms of densities or by using positivity-preserving flux limiters. Boundedness of fractions is maintained through a transformed-variable representation, such as evolving θ_α and θ_d where $\alpha_g = \sigma(\theta_\alpha)$ and $x_d = \sigma(\theta_d)$ [28]. This transformation makes the invariant region automatic, but it changes the conservative structure. To preserve conservation where it matters, the scheme evolves conservative masses and reconstructs fractions through a constrained solve that respects bounds. In practice, free-gas mass and dissolved-gas mass are conserved variables, and the corresponding fractions are computed from these masses and densities. This avoids direct transport of α_g and x_d as primary variables, reducing numerical diffusion that can otherwise smear phase appearance.

Dissolution exchange is stiff when κ_d is large, which

Table 5. Invariant-region constraints.

Variable	Bounds	Enforcement
ρ_g	> 0	Positivity-preserving update / log form
ρ_l	> 0	$B_l \geq 1$ and bounded x_d
α_g	$0 \leq \alpha_g \leq 1$	Conservative masses, constrained recon.
x_d	$0 \leq x_d \leq 1$	Bounded implicit relaxation
p	$[p_{\min}, p_{\max}]$	CFL, thermo table limits

Table 6. Calibrated parameter groups.

Group	Symbols	Main effect
Friction	c_f, θ_f	Distributed pressure loss, smoothing
Slip	θ_s	Gas rise speed and migration timing
Dissolution	κ_d	Rate toward $x_d^\star(p, T)$
Swelling	β_1, β_2	Volume change vs. x_d
Thermo props	M_g, Z surrogate	Gas density and wave speeds
Biases	$b_{\mathrm{SP}}, b_{\mathrm{C}}, b_{\mathrm{pit}}$	Sensor offsets in data fit

can destabilize explicit updates and can produce negative free-gas mass when equilibrium strongly favors dissolution [29]. The scheme therefore uses an IMEX operator split. The transport and non-stiff sources are advanced explicitly with the entropy-stable flux, while the dissolution source is advanced implicitly in each cell, holding transport fluxes fixed over the substep. In each cell, the implicit update preserves total gas inventory and maps free and dissolved masses to new values consistent with equilibrium. Because the dissolution update is local, it is computationally cheap, and because it is monotone, it preserves positivity [30].

A representative implicit update for dissolved fraction can be written in terms of dissolved-gas mass $m_d = \alpha_l \rho_l x_d$ and free-gas mass $m_g = \alpha_g \rho_g$. The exchange conserves $m_d + m_g$ aside from influx. The relaxation source yields a linear implicit equation in x_d when ρ_l is held fixed over the substep, but ρ_l depends on x_d through swelling. The paper treats this dependence by solving a scalar nonlinear equation per cell with a safeguarded Newton method, using the boundedness of x_d to guarantee convergence. The solver is differentiable through an implicit function theorem treatment, described later, ensuring that gradients do not depend on the number of Newton iterations [31].

Entropy stability interacts with differentiability through the choice of limiters and dissipation scaling. Traditional total-variation-diminishing limiters are non-smooth, producing discontinuous gradients that complicate calibration. The present method uses smooth limiting functions that approximate TVD behavior while remaining differentiable. The entropy inequality provides an additional safeguard by controlling oscillations even when the limiter is softened for differentiability, reducing the reliance on hard clipping [32].

The net effect of these design choices is a discretization that remains stable under transient actuation, avoids unphysical states, and produces forward trajectories that are sufficiently regular for meaningful sensitivity analysis. The next section leverages this differentiability to develop an adjoint-based calibration approach for uncertain parameters and sensor biases.

4. Adjoint-Based Calibration with Differentiable IMEX Updates

Online calibration in drilling hydraulics must operate with limited and noisy data, and it must avoid conflating model mismatch with influx inference. A calibration mechanism that adjusts uncertain parameters, such as friction multipliers, slip coefficients, dissolution kinetics, and sensor biases, can reduce systematic residuals and improve both prediction and interpretation. Adjoint methods provide an efficient route to such calibration because they compute gradients of a scalar objective with respect to many parameters at a cost largely independent of parameter dimension, provided the model is differentiable [33].

Let the discrete-time simulator over a window $n = 0, \ldots, N$ be written as

$$X_{n+1} = \mathcal{M}(X_n, U_n; \theta) \tag{13}$$

where X_n is the discrete state vector, U_n are known inputs such as pump and choke signals, and θ are parameters. Let observations be $Y_n = \mathcal{H}(X_n; \theta)$ compared against measured data $\tilde{Y}_n$. A calibration objective is

$$J(\theta) = \frac{1}{2} \sum_{n=0}^{N} |0\mathcal{H}(X_n; \theta) - \tilde{Y}_n|0^2_{R^{-1}} + \frac{1}{2} |0\theta - \theta_0|0^2_{P_0^{-1}} \tag{14}$$

Table 7. Measurement channels for calibration.

Channel	Symbol	Dominant sensitivity
Standpipe pressure	$p_{\mathrm{SP}}(t)$	Friction, inlet compressibility
Casing / annulus pressure	$p_{\mathrm{C}}(t)$	Hydrostatics, choke moves, influx depth
Flow-in	$Q_{\mathrm{in}}(t)$	Pump schedule, inlet density
Flow-out	$Q_{\mathrm{out}}(t)$	Near-surface gas and swelling
Pit volume	$V_{\mathrm{pit}}(t)$	Net volume, dissolution-driven gain

Table 8. Representative numerical scenarios.

Case	Regime	Focus
A	No influx, choke steps	Entropy damping of pressure waves
B	Strong dissolution	Early pit gain with low gas rate
C	Free-gas dominated	Sharp fronts and pit response timing
D	Property perturbation	Friction vs. gas-property trade-off
E	Stiff dissolution + actuation	Adjoint stability and gradients

where R weights measurement residuals and the second term encodes a prior or regularization around θ_0 with covariance-like weight P_0 [34]. The prior is important because some parameters are weakly identifiable from surface data without deliberate excitation.

The discrete adjoint method introduces Lagrange multipliers Λ_n enforcing the dynamics. The Lagrangian is

$$\mathcal{L} = J(\theta) + \sum_{n=0}^{N-1} \Lambda_{n+1}^{\top}\big(X_{n+1} - \mathcal{M}(X_n, U_n; \theta)\big) \tag{15}$$

Setting derivatives with respect to X_n to zero yields the adjoint recursion, which runs backward in time. The gradient of J with respect to θ is then computed from the adjoint variables and the partial derivatives of $\mathcal{M}$ and $\mathcal{H}$ with respect to θ.

The challenge in this application is that $\mathcal{M}$ includes an implicit dissolution update and smooth limiters. Differentiating through an implicit update by unrolling Newton iterations can be unstable and iteration-dependent [35]. The present approach treats the implicit substep as a mapping defined by a root condition. In each cell, the implicit update solves $G(x_d^{n+1}, \cdot) = 0$ for x_d^{n+1}, where G encodes the implicit relaxation and swelling coupling. Under mild conditions, the implicit function theorem implies that

$$\frac{\partial x_d^{n+1}}{\partial \vartheta} = -\Big(\frac{\partial G}{\partial x_d^{n+1}}\Big)^{-1} \frac{\partial G}{\partial \vartheta} \tag{16}$$

for any variable or parameter ϑ that influences G. This derivative can be computed using the same Jacobian factor already computed in Newton's method, without unrolling iterations [36]. Because $\partial G/\partial x_d^{n+1}$ is scalar and bounded away from zero by design, the derivative is stable. This treatment yields consistent gradients and improves adjoint conditioning when κ_d is large.

Entropy-stable fluxes contribute to adjoint stability by preventing high-frequency oscillations that would otherwise make $\mathcal{H}(X_n)$ highly sensitive to small parameter changes in nonphysical ways. In calibration, this matters because the objective gradients should reflect meaningful physical sensitivities, such as how friction changes alter pressure drop, rather than how numerical ringing shifts a local pressure node. The entropy inequality acts as a numerical regularizer that is consistent with the physics of dissipation, avoiding ad hoc smoothing that could distort inference.

Parameter choices include friction multipliers, slip parameters, dissolution kinetics κ_d, swelling coefficients β_1 and β_2, and sensor biases. Sensor biases are treated as parameters in θ with slow evolution or constant over the window [37]. Including bias parameters is essential when calibrating against pit volume, where tank calibration and flow meter offsets can induce persistent residuals. Without bias modeling, an optimizer can incorrectly attribute bias to dissolution or to influx, corrupting the inferred gas inventory.

The calibration window can be updated in a receding-horizon manner. At each update, a short history is used to compute a gradient and update θ using a quasi-Newton step. Because the simulator is stable, modest step sizes can be used without destabilizing the forward model [38]. The calibrated parameters then inform both prediction and any downstream influx inference. The paper emphasizes that calibration and influx estimation should not be conflated: calibration reduces systematic residuals that are explainable by parameter shifts, while residuals that remain after calibration are more plausibly attributable to unmodeled disturbances such as influx.

Table 9. Implementation choices relevant for real-time use.

Aspect	Design choice	Benefit
Time stepping	Multirate CFL transport	Capture waves with modest cost
Dissolution solve	Local implicit, IFT derivative	Stable and differentiable update
Thermodynamics	Smooth monotone tables for $Z, x_d^\star$	Physical bounds and gradients
Boundary actuation	Smooth choke/pump maps	No hard kinks in sensitivities
Checkpointing	Interval-based with recompute	Adjoint feasible in memory

A practical identifiability issue arises between dissolution kinetics and slip. Both can affect the timing of surface signatures [39]. The calibration framework addresses this by incorporating multiple measurement channels, such as casing pressure, standpipe pressure, flow-out, and pit-volume change, and by weighting these channels to reflect their relative reliability. Pressure signals are more directly influenced by friction and density, while pit signals are influenced by swelling and volumetric mapping. The combination helps separate effects, though complete identifiability is not guaranteed in all operating conditions. The method therefore maintains regularization and bounds on parameters to prevent unphysical calibrated values that would fit noise.

To formalize the role of entropy stability in conditioning, consider that the adjoint recursion involves Jacobians of the forward mapping [40]. If the forward scheme produces oscillations, these Jacobians can have large norms, leading to exploding adjoints and unreliable gradients. Entropy-stable dissipation reduces these norms by damping high-frequency modes in a controlled way, keeping Jacobians closer to those of the underlying physical system rather than those of a numerically unstable discretization. This improves gradient reliability under aggressive actuation, which is precisely the regime where calibration is most valuable because excitation is present.

The next section discusses implementation choices that enable these computations under real-time constraints, including multirate stepping, differentiable interpolation for thermodynamics, and computational strategies that preserve stability while limiting latency [41].

5. Multirate Real-Time Implementation and Differentiable Thermodynamic Evaluation

A simulator suitable for calibration and decision support must deliver trajectories and gradients within operational time budgets. The computational challenge is shaped by stiffness separation: pressure waves and boundary actuation can evolve on time scales smaller than gas migration, while dissolution exchange can be stiff relative to transport. A uniform time step chosen for the fastest process would be inefficient. The implementation therefore adopts a multirate approach in which fast dynamics are integrated with smaller substeps while slow dynamics are advanced with larger steps, maintaining consistency and differentiability.

The finite-volume transport update uses a CFL-limited time step based on characteristic speeds [42]. During periods of aggressive choke actuation, this time step can become small. However, for calibration over a window, it is not necessary to resolve every pressure wave with equal fidelity if the measurement sampling is coarser. The implementation therefore integrates pressure and mixture momentum with substeps within a measurement interval, while transporting gas inventory and dissolved fraction with a larger step that preserves conservation. The coupling is handled through operator splitting that is designed to preserve entropy stability at the outer step and to maintain consistent state updates for the adjoint [43].

Dissolution exchange is advanced implicitly within each outer step. Because the implicit solve is local, it scales linearly with the number of cells and can be parallelized. The key for differentiability is to ensure that the implicit solver returns not only the updated state but also the local derivative factors required by the implicit function theorem. These factors are stored and used during the adjoint sweep, reducing recomputation and ensuring that the gradient is consistent with the forward update.

Thermodynamic evaluation is performed through tabulated mappings for $Z(p, T)$ and $x_d^\star(p, T)$ [44]. Direct table lookup is fast, but naive interpolation can be non-differentiable at cell boundaries or can violate monotonicity. The implementation uses smooth interpolation with monotone constraints, ensuring that Z and $x_d^\star$ remain within physical bounds and that derivatives exist. The interpolation is implemented as a differentiable operator that returns both values and partial derivatives with respect to p and T, which are needed for the adjoint.

Temperature is treated as a known profile or as a bounded estimate [45]. When a temperature model is used, it is low-order and smooth, avoiding sharp switching behavior. The influence of temperature on solubility is then captured through the thermodynamic mapping. This choice is motivated by observability: surface measurements seldom constrain a high-dimensional temperature field directly, so a conservative and smooth representation is preferable for calibration stability.

Boundary conditions for choke and pump are represented as smooth functions of control signals and flows. Choke pressure drop is modeled as a differentiable function that is monotone in flow and smooth in choke opening [46]. If the choke model includes saturation or deadband, these are approximated by smooth saturations rather than hard clipping. This ensures that gradients exist and that the adjoint does not encounter discontinuities when the choke crosses a threshold. Similarly, pump dynamics and flow measurement lags are represented by smooth first-order filters.

An important implementation detail concerns the preservation of invariant regions under floating-point roundoff and under multirate coupling [47]. Even with theoretically invariant-preserving updates, roundoff can produce slight negativity in masses or fractions that then propagates. The implementation avoids explicit clipping because clipping destroys differentiability. Instead, it uses logarithmic and sigmoid parameterizations internally for quantities that must remain positive or bounded, and it reconstructs conservative masses through differentiable transformations. This yields a simulator that stays physically admissible without nondifferentiable projections.

Computationally, the most expensive part of adjoint calibration is the backward sweep, which requires access to intermediate states or to checkpointing [48]. The implementation uses checkpointing aligned with measurement intervals to limit memory. Within each interval, the forward substeps are recomputed during the backward sweep if needed. Because the substep integrator is explicit and cheap, recomputation is acceptable, and it avoids storing large arrays. The implicit dissolution factors are stored because they are local and cheap to store, and because recomputing them would require additional Newton iterations that can introduce numerical variability.

The simulator is thus structured as a differentiable program with controlled numerical regularity [49]. Its stability is not an incidental property but a design goal, enabling gradients that are meaningful for calibration. The next section evaluates the resulting method in numerical studies, focusing on entropy stability under actuation, the effect of dissolution-driven swelling on surface signatures, and the conditioning of gradients used for parameter updates.

6. Numerical Studies: Transient Actuation, Swelling Ambiguity, and Gradient Conditioning

The numerical studies are designed to test properties that matter for real-time calibration and interpretation rather than solely for offline accuracy. The main questions are whether the entropy-stable scheme suppresses nonphysical oscillations under aggressive boundary forcing, whether dissolution and swelling representation changes the interpretation of early pit signals in a controlled manner, and whether adjoint gradients remain stable across regimes where phase appearance and stiff dissolution would typically cause sensitivity blow-up [50].

A representative annulus geometry is selected with length and hydraulic diameter consistent with managed pressure drilling scenarios. The inlet pump schedule includes step and ramp changes to excite the system, and the choke schedule includes rapid adjustments that generate pressure waves and transient reversals in near-surface flow conditions. Influx scenarios are included with varying onset times and depths, and the dissolution strength is varied through the equilibrium mapping and swelling coefficients. Measurement channels include casing pressure, standpipe pressure, flow-in, flow-out, and pit-volume change, with noise and bias consistent with practical sensor characteristics.

The first study isolates numerical stability under choke actuation without influx [51]. In this setting, the correct physical response is a pressure transient that propagates and damps due to friction and compressibility, with negligible pit gain aside from compressibility-induced volumetric effects. A non-entropy-stable discretization can produce oscillatory pressure nodes that persist and that manifest as spurious flow-out oscillations. In the proposed scheme, the entropy-stable dissipation damps these high-frequency modes while preserving the main transient structure. The well-balanced gravity discretization prevents spurious drift in hydrostatic pressure, which is important because small hydrostatic errors can integrate to large bottomhole pressure deviations over long intervals [52].

The second study examines a dissolution-dominated early influx. A small mass influx occurs at depth under high pressure, and due to strong solubility and moderate kinetics, much of the gas dissolves, increasing swelling and reducing liquid density. The surface pit-volume change exhibits an early rise, but the surface gas fraction remains low. A model without dissolution would interpret the pit rise as free gas and would predict a corresponding surface gas risk earlier than observed. The proposed model produces a partition of gas inventory that yields pit rise driven primarily by swelling and predicts delayed free-gas appearance, consistent with the constructed scenario [53]. The emphasis here is not that the model eliminates ambiguity, but that it represents the ambiguity within a physically consistent state, enabling calibration and interpretation to separate swelling-induced volume change from free-gas expansion.

The third study examines a free-gas-dominated influx where solubility is weak or kinetics are slow. In this case, pit gain and pressure signatures are driven by free-gas holdup and migration. The simulator captures this regime through the same equations without special switching, and the entropy-stable flux handles the sharper fronts that can occur when free gas forms a

high-gradient region [54]. The invariant-region preservation prevents negative phase fractions during these transients, which is important because even slight negativity can corrupt derived quantities such as gas fraction at surface.

The fourth study focuses on calibration and gradient conditioning. Parameters include a friction multiplier, a slip coefficient, a dissolution kinetic coefficient, swelling coefficients, and a pit bias term. The objective combines pressure and pit residuals over a calibration window. The adjoint gradients are examined under varying time steps and under differing actuation aggressiveness [55]. Without entropy stability, gradients exhibit spikes correlated with numerical oscillations in pressure nodes, leading to unstable parameter updates that can overshoot and degrade fit. With entropy stability, gradients are smoother and align with physically interpretable sensitivities, such as increased friction reducing flow-out for a given pump schedule and increasing standpipe pressure.

A key gradient-conditioning test occurs near equilibrium dissolution, where x_d is close to $x_d^\star(p, T)$ and small pressure changes can change $x_d^\star$ rapidly. In explicit updates, this can create large local sensitivity because the discrete update can overshoot equilibrium and require clipping, which is non-differentiable [56]. In the present IMEX implicit update, the mapping from pressure to dissolved fraction is smooth and bounded, and the implicit-function-theorem derivative remains finite as long as the implicit Jacobian is bounded away from zero, which is ensured by design through the relaxation form and swelling bounds. As a result, gradients with respect to κ_d and swelling coefficients remain stable even when κ_d is large.

The studies also consider the interaction between property uncertainty and calibration. When gas density mapping is perturbed within a few percent, pressure residuals emerge that can be partially compensated by friction changes if calibration is unconstrained, leading to parameter trade-offs. Regularization and multi-sensor weighting reduce this tendency [57]. The calibrated parameters are assessed by cross-validating on a held-out interval. The entropy-stable scheme reduces the risk that calibration overfits numerical artifacts because the artifacts are suppressed in the first place, so the remaining residuals are more plausibly attributable to parameter mismatch or to unmodeled disturbances.

The numerical studies are not intended to claim universal superiority over all other modeling approaches, but to demonstrate that entropy stability and differentiability can be combined constructively in a dissolution-affected drilling hydraulics context. The main operational implication is that a simulator designed for both forward stability and sensitivity stability can support systematic calibration without sacrificing physical admissibility, reducing the likelihood that inference algorithms attribute numerical error to physical influx [58].

7. Conclusion

This paper developed an entropy-stable, invariant-region-preserving, and differentiable annular simulator for dissolution-affected gas influx dynamics in managed pressure drilling. The model incorporated a conserved decomposition of gas inventory into free and dissolved components, a bounded thermodynamic equilibrium mapping, and a swelling-induced modification of liquid density that influences hydrostatics and pit-volume behavior. The numerical method combined entropy-stable finite-volume fluxes with a well-balanced gravity discretization and an IMEX split for stiff dissolution exchange, producing forward trajectories that are robust under aggressive boundary actuation and that remain physically admissible without non-differentiable clipping.

The technical contribution was the integration of this stable forward method with adjoint-based calibration, enabled by differentiable fluxes and an implicit-function-theorem treatment of the implicit dissolution update. This design stabilized gradients in regimes where phase appearance and near-equilibrium dissolution would otherwise generate sensitivity pathologies [59]. The resulting calibration framework supports systematic adjustment of uncertain friction, slip, dissolution kinetics, swelling coefficients, and sensor bias, reducing systematic residuals that can otherwise bias influx inference.

Numerical studies demonstrated that entropy stability suppresses spurious oscillations under choke maneuvers, that dissolution-driven swelling can be represented as an internal state shaping pit and pressure signatures, and that stable gradients enable reliable parameter updates across both dissolution-dominated and free-gas-dominated regimes. The approach remains subject to limitations typical of control-oriented one-dimensional models, including simplified slip and friction closures and reliance on tabulated thermodynamic mappings. Future work can extend the framework toward richer thermal coupling, improved regime-adaptive slip representations that remain differentiable, and tighter coupling between calibration and uncertainty quantification. Within these bounds, the presented formulation provides a principled path to combine thermodynamic dissolution effects with numerically stable and differentiable simulation, supporting real-time calibration and more reliable interpretation of ambiguous early influx signals [60].

References

[1] A. Tallin, P. Paslay, E. P. Cernocky, and M. A. Ratchinsky, "Risk assessment of exploration well designs in the oman ara salt," in SPE Annual Technical Conference and Exhibition, SPE, 10 2000.

[2] V. Pipicz, L. Benedek, G. Palasthy, T. Barodi, J. Blaho, and S. Joshi, "The fourth horizontal project in the mature

algyo field," in SPE International Thermal Operations and Heavy Oil Symposium and International Horizontal Well Technology Conference, SPE, 11 2002.

[3] A. E. Omrani, M. A. Franchek, and Y. Tang, "Bop pressure and flowrate conditions during high pressure gas kick control," in Offshore Technology Conference, OTC, 4 2019.

[4] K. Manikonda, A. R. Hasan, O. Kaldirim, N. Rahmani, and M. A. Rahman, "Estimating swelling in oil-based mud due to gas kick dissolution," in International conference on offshore mechanics and arctic engineering, vol. 84430, p. V011T11A039, American Society of Mechanical Engineers, 2020.

[5] K. Manikonda, A. R. Hasan, N. H. Rahmani, O. Kaldirim, C. E. Obi, J. J. Schubert, and M. A. Rahman, "A gas kick model that uses the thermodynamic approach to account for gas solubility in synthetic-based mud," in SPE/IADC Middle East drilling Technology conference and exhibition, p. D031S016R001, SPE, 2021.

[6] S. Krueger, K. Gray, and D. Killip, "Fifteen years of successful coiled tubing re-entry drilling projects in the middle east - driving efficiency and economics in maturing gas fields," in SPE/IADC Middle East Drilling Technology Conference & Exhibition, SPE, 10 2013.

[7] A. K. Sleiti, W. A. Al-Ammari, M. Abdelrazeq, M. El-Naas, M. A. Rahman, A. Barooah, R. Hasan, and K. Manikonda, "Comprehensive assessment and evaluation of correlations for gas-oil ratio, oil formation volume factor, gas viscosity, and gas density utilized in gas kick detection," Journal of Petroleum Science and Engineering, vol. 207, p. 109135, 2021.

[8] K. Bybee, "Behavior and shape of gas kicks in wellbores," Journal of Petroleum Technology, vol. 63, pp. 71–72, 1 2011.

[9] A. Müller, E. Diemann, S. Q. N. Shah, C. Kuhlmann, and M. C. Letzel, "Soccer-playing metal oxide giant spheres: a first step towards patterning structurally well defined nano-object collectives.," Chemical communications (Cambridge, England), pp. 440–441, 3 2002.

[10] A. Torsvik, J. O. Skogestad, and H. Linga, "Impact on oil-based drilling fluid properties from gas influx at hpht conditions," IADC/SPE Drilling Conference and Exhibition, 3 2016.

[11] H. Mongia, K. Ajmani, and C.-J. Sung, Fundamental Combustion Research Challenged to Meet Designers' Expectations, pp. 251–285. United States: Springer Singapore, 9 2020.

[12] S. Ray and S. D. S. Sinha, "Non-equilibrium dynamics of quantum many body systems: Application to ultracold atomic gases," 5 2019.

[13] J. M. Gundlach, Section 115 in practice. Edward Elgar Publishing, 10 2020.

[14] J. E. Chirinos, J. R. Smith, and D. A. Bourgoyne, "Alternative shut-in and pump start-up procedures for kicks taken during mpd operations," in IADC/SPE Managed Pressure Drilling and Underbalanced Operations Conference & Exhibition, SPE, 4 2011.

[15] G. G. Wei and C. L. Kalloo, "The successful platform development of a gas field offshore the east coast of trinidad," in Latin American and Caribbean Petroleum Engineering Conference, SPE, 8 1997.

[16] X. Sun, B. Sun, and Z. Wang, "Wellbore dynamics of kick evolution considering hydrate phase transition on gas bubbles surface during deepwater drilling," in Volume 8: Polar and Arctic Sciences and Technology; Petroleum Technology, American Society of Mechanical Engineers, 6 2017.

[17] S. Tiwari, "Making a flow check to verify a kick can cause extra risks," Oil & Gas Journal, vol. 93, 11 1995.

[18] I. O. Sule, "Safety and reliability assessment of managed pressure drilling in well control operations," 7 2019.

[19] M. Shirdel and K. Sepehrnoori, "Development of a transient mechanistic two-phase flow model for wellbores," in SPE Reservoir Simulation Symposium, pp. 1389–1409, SPE, 2 2011.

[20] B. Hamoudi, K. Kartobi, H. H. Qutob, P. Vieira, M. A. Saad, and F. Torres, "Drilling hazard mitigation technology enables conventionally undrillable prospects to be drilled with reduced non-productive time and increased operational safety: Application of solid expandable liners and managed pressure drilling in algeria nezla field," in North Africa Technical Conference and Exhibition, SPE, 2 2012.

[21] J. Mathews and A. Bourgoyne, "How to handle a gas kick moving up a shut-in well," 12 1983.

[22] K. K. Nassab, S. Z. Ting, S. Buapha, N. MatNoh, and M. N. Hemmati, "More insight into kick tolerance calculations, and effect of kick classification, frictional losses, pore pressure profile and influx temperature," in SPE Asia Pacific Oil & Gas Conference and Exhibition, SPE, 11 2020.

[23] D. Zbinden, "Reply to review comment 2," 4 2020.

[24] S. Irawan, I. Kinif, M. T. Fathaddin, and Z. B. Zakaria, "Implication of the multiphase influx in well control and circulating system," Journal of Earth Energy Science, Engineering, and Technology, vol. 3, 2 2020.

[25] K. Bybee, "Simulation and analysis of a shallow gas kick," Journal of Petroleum Technology, vol. 53, pp. 40–41, 1 2001.

[26] N. Eddy, B. Fellenz, P. Prieto, A. Semenov, D. Voy, and M. Wendt, "A wire position monitor system for the 1.3 fhz tesla-style cryomodule at the fermilab new-muon-lab accelerator," 8 2011.

[27] D. Sasongko, G. R. Darmawan, S. D. Susilo, J. T. Shaun, S. Sisworo, and A. E. Prasetia, "Downhole isolation valve performance in drilling and subsequent completion operations," in International Petroleum Technology Conference, IPTC, 11 2011.

[28] S. Kumar, "Internal structure of hydrated sediments and bsr as seismic evidence of free gas trapping by hydrate zone," in Offshore Technology Conference, OTC, 5 1998.

[29] J. Merryman, "Estimating gas kick arrival to better manage surface flow," 6 1997.

[30] R. A. Shishavan, C. Hubbell, H. D. Perez, J. D. Hedengren, D. S. Pixton, and A. P. Pink, "Multivariate control for managed pressure drilling systems using high speed telemetry," in SPE Annual Technical Conference and Exhibition, SPE, 10 2014.

[31] B. Kayael, "Ultra-deep offshore well casing design process," 5 2011.

[32] B. Sun, G. Peibin, and Z. Wang, "Simulation of gas kick with high h2s content in deep well," Journal of Hydrodynamics, vol. 25, pp. 264–273, 4 2013.

[33] Y.-J. Xu, "Selective oxidation of hydrocarbons using supported gold, silver, copper and bimetallic catalysts," 9 2006.

[34] O. C. Michael, I. S. Ugochukwu, O. Boniface, A. Chibunma, and N. Stephen, "A realistic kick simulator for casing design-part 1," in SPE Nigeria Annual International Conference and Exhibition, SPE, 7 2017.

[35] B. Boyce, C. Harr, and L. Burch, "Saga of coal bed methane, ignacio blanco gas field, colorado," AAPG Bulletin, 9 1989.

[36] N. Fuda, L.-N. Tram, and W. T. Reach, "Modeling co line profiles in shocks of w28 and ic44," 12 2021.

[37] P. L. O'Bryan, A. T. Bourgoyne, T. G. Monger, and D. P. Kopcso, "An experimental study of gas solubility in oil-based drilling fluids," SPE Drilling Engineering, vol. 3, pp. 33–42, 3 1988.

[38] J. Ji, S. Jin, and C. G. Tinney, "Forming close-in earth-like planets via a collision-merger mechanism in late-stage planet formation," The Astrophysical Journal, vol. 727, pp. L5–, 12 2010.

[39] S. Orusa, "Career captain drowns after running out of air during technical rescue scuba dive - north carolina.," 12 2021.

[40] E. P. Andersson, O. Agertz, and F. Renaud, "How runaway stars boost galactic outflows," Monthly Notices of the Royal Astronomical Society, vol. 494, pp. 3328–3341, 4 2020.

[41] J. Orban, M. Dennison, B. Jorion, and J. Mayes, "New ultrasonic caliper for mwd operations," SPE/IADC Drilling Conference, 3 1991.

[42] V. Casariego, "Generation, migration, and transportation of gas contaminated regions of drilling fluid.," 1 1987.

[43] T. Zoete, "Biodiversity offsetting: implications for the oil and gas industry in australia," The APPEA Journal, vol. 50, pp. 187–202, 6 2010.

[44] P. O'bryan, "Well control problems associated with gas solubility in oil-based drilling fluids.," 1 1988.

[45] C. Bøe, M. Hjelmeland, and B. H. Torkildsen, "Gullfaks subsea compression: Early operational experience from the world's first subsea wet gas compression system," in Offshore Technology Conference, OTC, 4 2018.

[46] E. H. Vefring, Z. Wang, R. Rommetveit, and G. F. Bach, "An advanced kick simulator for high angle and horizontal wells - part ii," SPE/IADC Drilling Conference, 2 1995.

[47] Y. Liao, Z. Wang, D. Pan, B. Sun, and W. Duan, "Gas kick simulation for offshore gas-hydrate reservoir drilling," in Abu Dhabi International Petroleum Exhibition & Conference, SPE, 11 2019.

[48] A. Askar, M. B. Davies, and R. P. Church, "Formation of supermassive black holes in galactic nuclei ii: retention and growth of seed intermediate-mass black holes," 7 2021.

[49] G. R. Darmawan, S. D. Susilo, and J. S. S. Toralde, "Ssuccessful installation and operation of downhole isolation valve combined with pressurized mud cap drilling to safely develop sour gas, fractured-limestone reservoir in gundih field, indonesia," in SPE European Health, Safety and Environmental Conference in Oil and Gas Exploration and Production, SPE, 2 2011.

[50] M. Jellison and E. Klementich, "An expert system for casing string design," in Petroleum Computer Conference, SPE, 6 1990.

[51] A. Dasari and J. Njuguna, "Introduction," 6 2016.

[52] E. N. Monteiro, P. Ribeiro, and R. F. T. Lomba, "Study of the pvt properties of gas - synthetic drilling fluid mixtures applied to well control operations," in SPE Annual Technical Conference and Exhibition, SPE, 9 2008.

[53] A. Santos and O. Luiz, "Technology focus: Well integrity and well control (january 2018)," Journal of Petroleum Technology, vol. 70, pp. 58–58, 1 2018.

[54] H. Kang, Y. Takahashi, and H. Kakizaki, "Migration of rigid gas permeable contact lens into the upper eyelid after trauma: a case report," BMC ophthalmology, vol. 16, pp. 71–71, 6 2016.

[55] C. Tian, A. Kamenev, and A. I. Larkin, "Weak dynamical localization in periodically kicked cold atomic gases.," Physical review letters, vol. 93, pp. 124101–, 9 2004.

[56] W. E. S. Vielma, R. Quijada, D. Feltracco, V. Mittiga, I. Mosti, and K. Nergaard, "Increasing drilling operational margins of an onshore mature field in pakistan by including a dynamic drilling modeling approach," SPE Europec featured at 79th EAGE Conference and Exhibition, 6 2017.

[57] R. Rommetveit, K. Bjorkevoll, G. Bach, B. Aas, J. HyBilliot, R. Maglione, and P. Gie, "Full scale kick experiments in horizontal wells," SPE Annual Technical Conference and Exhibition, 10 1995.

[58] E. Saeverhagen, C. Erichsen, A. K. Nesheim, and G. Waldron, "3d rss for 24-in. section sets inclination record on the grane field by introduction of an integrated drilling and surveying bottomhole assembly," in SPE Annual Technical Conference and Exhibition, SPE, 9 2008.

[59] Y. Liu, Z. Wu, Y. Wang, Y. Xiao, F. Gu, J. Zheng, T. Tan, D. Shang, Y. Wu, L. Zeng, M. Hu, A. P. Bateman, and S. T. Martin, "Submicrometer particles are in the liquid state during heavy haze episodes in the urban atmosphere of beijing, china," Environmental Science & Technology Letters, vol. 4, pp. 427–432, 9 2017.

[60] L. Wei, S. Lin, Y. Zhou, W. Ying, and H. Jiang, "Development and application of pressure control drilling system (pcds) for drilling complex problem," in International Petroleum Technology Conference, IPTC, 3 2013.